INVESTIGATION ON THE EFFECT OF ESTUARY SHAPE IN PROPAGATING SALINITY INTRUSION

JACQUELINE ISABELLA GISEN

RESEARCH VOTE NO:
RDU151112

Faculty of Civil Eng. and Earth Resources
Universiti Malaysia Pahang

2017

ACKNOWLEDGEMENTS

I am grateful and would like to express my deepest appreciation to all those who provided me with the possibility to complete this research. A special gratitude to give to my former supervisor, Prof. Dr. Ir. Hubert Savenije from Delft University of Technology. His willingness in working together to make this research a success is highly appreciated.

I would also like to acknowledge with much appreciation Dr. Ali D. Abdullah from IHE Delft for his interest to adopt this research outcome (newly developed equation) in his research. Consequently, a joint publication is achieved.

Last but not least, my gratitude goes to Universiti Malaysia Pahang (UMP) for the funding support through grants number RDU151112, Centre for Earth Resources Research Management (CERRM) and other technical members for their invaluable support and assistance in completing the fieldworks; and the Department of Irrigation and Drainage (DID) Malaysia for providing the hydrological data.

ABSTRACT

For one-dimensional salt intrusion models to be predictive, we need predictive equations to link model parameters to observable hydraulic and geometric variables. The one-dimensional model of Savenije (1993b) made use of predictive equations for the Van der Burgh Coefficient K and the dispersion at the seaward boundary D_0. Here we have improved these equations by using an expanded database, including new previously un-surveyed estuaries. Furthermore, we derived a revised predictive equation for the dispersion at tidal average condition and with the boundary situated at the well identifiable inflection point where the estuary changes from wave-dominated to tide-dominated geometry. We used 89 salinity profiles in 30 estuaries (including seven recently studied estuaries in Malaysia), and empirically derived a range of equations using various combinations of dimensionless parameters. We split our data in two separated data sets: (1) with more reliable data for calibration, and (2) with less reliable data for validation. The dimensionless parameters that gave the best performance depended on the geometry, tidal strength, friction and the Richardson number. The limitation of the equations is that the friction is generally unknown. In order to overcome this problem, a coupling has been made with the analytical hydraulic model of Cai et al. (2012), which makes use of observed tidal damping and by which the friction can be determined.

TABLE OF CONTENT

LIST OF TABLES

LIST OF FIGURES

LIST OF SYMBOLS

A	Cross-sectional area, m^2
A_0	Cross-sectional area at estuary mouth, m^2
A_1	Cross sectional area at inflection point, m^2
a_1	Cross-sectional convergence length of the seaward reach of estuary, m
a_2	Cross-sectional convergence length of the landward reach of estuary, m
B	Estuary width, m
B_0	Width at estuary mouth, m
B_1	Width at inflection point x_1,m
b_1	Width convergence length of the seaward reach of estuary, m
b_2	Width convergence length of the landward reach of estuary, m
C	Runoff coefficient (dimensionless)
D	Dispersion boundary condition
D	Longitudinal dispersion, m^2s^{-1}
D_0	Longitudinal dispersion at estuary mouth, m^2s^{-1}
D_1	Longitudinal dispersion at inflection point x_1, m^2s^{-1}
E	Tidal excursion
g	gravitational force
K	Van der Burgh coefficient (range 0-1)
L	Salt intrusion length, km
Nr	Richardson number
S	Steady state salinity , kgm^{-3}
S_0	Steady state salinity at estuary mouth, kgm^{-3}
S_1	Salinity at inflection point , kgm^{-3}
S_f	Freshwater salinity, kgm^{-3}
T	Tidal period, s
t_c	Time of concentration of watershed
v	Velocity amplitude
x	Distance, m
x_1	Longitudinal distance, m
α_1	Mixing number at inflection point x_1, m^{-1}
α_0	Mixing number at estuary mouth, m^{-1}
β_0	Dispersion reduction rate at the estuary mouth (dimensionless)
β_1	Dispersion reduction rate at the inflection point x_1 (dimensionless)
ρ	Water density, kgm^{-3}
$\Delta\rho$	Density difference over the intrusion length,ms^{-2}

LIST OF ABBREVIATIONS

1-D	*One-Dimensional*
2-D	*Two-Dimensional*
3-D	*Three-Dimensional*
AD	*Advection Dispersion*
DID	*Department of Irrigation and Drainage Malaysia*
HWS	*High Water Slack*
LWS	*Low Water Slack*
TA	*Tidal Average*

CHAPTER 1

INTRODUCTION

1.1 Background of Study

Predictive methods to determine salinity profiles in estuaries can be very useful to water resources managers, particularly when applied to ungauged estuaries where only a minimal amount of data are available. Before any decision is made on collecting detailed field observations, it is useful to obtain a first estimate of the strength and range of the salt intrusion in the area of interest. Such estimate can be made if there are predictive equations available to compute the longitudinal salinity profile along the estuary. With reliable predictive equations, water managers are able to estimate how far salt water intrudes into the river system under different circumstances, and more importantly, how interventions may change this situation.

The one-dimensional salt intrusion model of Savenije (1993b) makes use of the Van der Burgh and dispersion equations to represent the longitudinal variation of the salinity. The Van der Burgh and dispersion coefficient at the ocean boundary are obtained by calibration of the simulated salinity curve to observations. Savenije (1993b) established a predictive equation for each of these parameters, so that the longitudinal salinity distribution could be estimated when data were lacking or to monitor the impact of interventions, such as dredging or fresh water withdrawal. The predictive equations have subsequently been modified and tested by several researchers including Savenije (2005), Nguyen and Savenije (2006), Kuijper and van Rijn (2011) and Shaha and Cho (2009).

In this paper, we shall revisit the predictive equations in the light of new insights on how friction and estuary shape affect tidal mixing by deriving a relationship between several governing parameters, making use of the salinity measurements from 30 estuaries

including seven new field observations in previously ungauged estuaries in Malaysia that were sampled through a consistent approach. As a result, we present the fully revised and more accurate predictive equations for the Van der Burgh coefficient and for the boundary value of the dispersion at a well identifiable location, based on tidal average (TA) condition.

1.2 Problem Statement

Managing estuaries can be very troublesome, especially in ungauged basins. Until today, most of the estuary basins worldwide are still ungauged except for some very large estuaries such as the Yangtze, Schelde, Elbe, Thames and others. Conducting field surveys to study an ungauged estuary is always time and energy consuming, and may be very expensive. Without substantial funding, it is almost impossible to collect the data needed to investigate the underlying hydrological processes in an estuary. Although some estuaries have been widely explored, there is still no comprehensive compilation of databases accessible for all the gauged estuaries. The only way to obtain the existing data for these estuaries is from the literature (e.g. Savenije (2005, 2012); Toffolon and Savenije (2009)).

Information on geometry such as cross-sectional areas of an estuary often requires intensive field surveys: either self-conducted or by professional surveyors and this can sometimes be very difficult. The hydrological data such as fresh water discharge on the other hand, can be collected from the authority of the countries to which the estuaries belong. However, the available streamflow stations are commonly situated further upstream from the upper boundary of the estuaries. This has led to the underestimation of the actual fresh water discharge draining into the estuaries. In salt intrusion models, regardless of being analytical or numerical 1-D, 2-D or 3-D models, at least two (e.g. the Van der Burgh Coefficient K and dispersion coefficient D_0) or more parameters have to be calibrated to fit the salinity curve against measured salinity data. This means that the longitudinal salinity distribution can be simulated only with the presence of salinity measurements. Savenije (1993a, 2005) provided predictive equations for K and D0, but these are subject to improvement.

Realizing the complications in conducting estuary studies, we have taken the initiative to search for possible methods to simplify the investigation process. This is done

by searching for new predictive methods to enable a further understanding of the hydrological processes in estuaries of interest. Improving the existing and developing new predictive tools would be very useful for water managers and engineers in managing estuaries.

1.3 Objectives of Study

The objectives of this research is:

1. To improve the current equation describing estuary geometry in which the revised version will be important for accurate salinity prediction in Malaysian estuaries, but also for world-wide application.

1.4 Scope of Study

The study area of this research covers the tidal region of estuaries from the mouth until the upstream of the related river to the point when the salinity reach zero level. Field measurements were carried out during the dry period at spring tide as salt intrusion is most crucial when there is the least of rainfall. It is worth to note that neap tide measurement was not considered in this study because the timing of the slack moment occurred at night time and during the dawn which make the field work impossible to conduct. This research required a considerable amount of data collection activities, including primary and secondary data 1) primary data: field observation data 2) secondary data: readily available topography and hydrological data. The topography map and hydrological data collected from secondary sources. Field observations data collected are the cross-sectional area (width and depth) and salinity data. Weighted area method combined with Geographic Information System (ArcGIS) were used in order to estimate freshwater discharge in the river basins. The digital elevation model (DEM) used in ArcGIS is the shuttle radar topography mission (SRTM) with 30m resolution. For the salt intrusion modelling, the geometry and salinity analyses were carried out by adopting the theory developed by Savenije (1986) which claimed that the cross-sectional area and width of an estuary can be expressed in an exponential function. Both the geometry and salinity analyses were performed in reference to tidally average condition. The 1D-

analytical salt intrusion model and its predictive equations was considered only for the steady state condition.

1.5 Significance of Study

Salt intrusion highly affects the water supply quality if the locations of water intake stations are not properly determined at the downstream region. The level of salinity distribution in the estuary is closely dependent on the amount of freshwater discharge in which the lower the discharge resultant in further salt intrusion limit. Since, the geometry of an estuary affects the hydrodynamics in the system, it is essential to seek for a simple yet useful method to estimate the river flow efficiently. Results from the analyses are important to ensure the suitability of water resources in any river basin term of quantity and quality for water supply activity.

CHAPTER 2

LITERATURE REVIEW

2.1 One-dimensional Analytical Salt Intrusion Model

The analytical one-dimensional salinity model developed by Savenije (1993b, 2005, 2012), presented below, is used to simulate the salinity profile in the estuaries studied. In a steady state situation, the partial temporal derivative in the salt balance equation is zero. Considering a constant fresh water discharge Q_f [L^3T^{-1}] and tidally averaged cross-sectional area A [L^3], the salt balance equation for tidal average (TA) condition can then be written as:

$$S - S_f = \frac{A}{|Q_f|} \cdot D \frac{dS}{dx} \qquad 2.1$$

where $S = S(x)$ [ML^{-3}] and $D = D(x)$ [L^2T^{-1}] are the salinity and dispersion at TA condition. Since discharge has a negative value, the absolute value of Q_f is taken in Equation (2.1). S_f [ML^{-3}] represents the fresh water salinity. In 1972, Van der Burgh derived an empirical equation for the TA dispersion making use of a large amount of salinity measurements in the Rotterdam Waterway. The equation is then revisited by Savenije (2005, 2012) who described the relation between dispersion and salinity to be:

$$\frac{dD}{dx} = -K\frac{|Q_f|}{A} \qquad 2.2$$

in which K [–] is defined as the Van der Burgh coefficient (shape factor). Substituting Equation (2.1) into Equation (2.2), the differential equation for the tidally averaged longitudinal salinity distribution is expressed as:

$$\frac{dS}{S - S_f} = \frac{1}{K}\frac{dD}{D} \qquad 2.3$$

Integration of Equation (2.3) leads to:

$$\frac{S - S_f}{S_0 - S_f} = \left(\frac{D}{D_0}\right)^{1/K} \quad 2.4$$

The symbols S [ML^{-3}] and D [L^2T^{-1}] are the steady state salinity and dispersion coefficient at location x, while S_0 [ML^{-3}] and D_0 [$L^2\ T^{-1}$] are the salinity and dispersion at the estuary mouth.

In alluvial estuaries, the variation of the estuaries shape over the distance upstream can be expressed in an exponential function (Savenije, 2005, 2012; Nguyen and Savenije, 2006; Zhang et al., 2011) as:

$$A = A_0 e^{-\left(\frac{x}{a}\right)} \quad 2.5$$

$$B = B_0 e^{-\left(\frac{x}{a}\right)} \quad 2.6$$

where a [L] and b [L] representing the cross-sectional area and width convergence length, A_0 [L^2] and B_0 [L] are the cross-sectional area and width at the mouth, B [L] is the width of estuary at distance x [L] (towards upstream). Substituting the exponential relation of Equation (2.5) into Equation (2.2) and the integration gives:

$$\frac{D}{D_0} = 1 - \beta\left[e^{\left(\frac{x}{a}\right)-1}\right] \quad 2.7$$

with,

$$\beta = \frac{Ka\left|Q_f\right|}{D_0 A_0} \quad 2.8$$

Here, β [–] is the dispersion reduction rate. At the salt intrusion limit (upstream) where only fresh water discharge exists, the dispersion coefficient becomes zero and x is equal to the salt intrusion length L [L]. Hence, the intrusion length is expressed by:

$$L = a \ln\left(\frac{1}{\beta} + 1\right) \qquad 2.9$$

Equations (2.4) to (2.9) are the general equations used to compute the longitudinal salinity distribution.

2.2 Existing Predictive Equations

Van der Burgh's coefficient K is also known as the "shape factor" in the salinity curve (Savenije, 1993a). Based on salinity measurements of 15 estuaries, Savenije found that K is strongly related to the geometry (the convergence length a or b and the width B [L]) and its influence is more significant at the tail of the salinity curve (upstream). Moreover, Savenije (1986, 1989) observed that every estuary had its own characteristic value of K, ranging from zero to one.

Assuming that the Van der Burgh coefficient is not time dependent, Savenije (1993b) established an empirical predictive equation for K as:

$$K = 0.16 \times 10^{-6} \frac{h_0^{0.69} g^{1.12} T^{2.24}}{H_0^{0.59} b^{1.10} B_0^{0.13}} \qquad 2.10$$

where h_0 [L], H_0 [L] and B_0 [L] are the depth, tidal range and width at the estuary mouth, respectively. The symbol T [T] represents the tidal period, while b [L] is the width convergence length, and g [LT^{-2}] is the gravity acceleration. More than 10 years later, Savenije (2005) and Nguyen and Savenije (2006) made used of an expanded database, modified the predictive equation involving more parameters:

$$K = 0.3 \times 10^{-3} \left(\frac{E}{H}\right)^{0.65} \left(\frac{E}{C^2}\right)^{0.39} (1 - \delta_H b)^{-2.0} \left(\frac{b}{a}\right)^{0.85} \left(\frac{Ea}{A'}\right)^{0.14} \qquad 2.11$$

The symbols E [L], H [L] and A_0 [L^2] refer to the tidal excursion, tidal range and a boundary value for the cross-sectional area, respectively. This relation had a correlation of 0.93 and seemed very promising. However, as can be seen from the equation, the Chezy roughness C [$L^{0.5}T^{-1}$] and damping δ_H [L^{-1}] had to be computed from tidal dynamics analysis.

2.3 Dispersion Coefficient

Dispersion is not a physical parameter; it is rather the product of averaging, representing the mixing of saline and fresh water in an estuary as a result of residual circulation induced by density gradients (gravitational circulation) and tidal movement. In salt intrusion modelling, the definition of dispersion is often unclear as it is scale dependent and not directly measurable. The role of dispersion is only meaningful if it is related to the appropriate temporal and spatial scale of mixing, which here we identify as the tidal period (timescale), tidal excursion (longitudinal mixing length), estuary width (lateral mixing length) and depth (vertical mixing length). A physically based description of the dispersion would allow the analytical solution of the salt intrusion profile. Dispersion due to gravitational circulation has been studied since 1957, as summarized by Fischer (1976). This type of dispersion is also known as density-driven dispersion between the two main sources: sea water and fresh river water.

Schultz and Simmons (1957) were some of the first to relate buoyancy to mixing in estuaries, whereby they introduced the ratio between fresh water discharge and tidal volume to represent the degree of stratification. This ratio is also known as the Canter–Cremers number N [–] as defined by Harleman and Abraham (1966). The buoyancy effect or stratification in an estuary can also be represented by the estuarine Richardson number N_r [–] which is the ratio of potential energy of the buoyant fresh water to the kinetic energy of the tide:

$$N_r = \frac{\Delta\rho}{\rho}\frac{gh}{\upsilon^2}\frac{Q_f T}{AE} \qquad 2.12$$

where ρ [ML^{-3}] is the water density, $\Delta\rho$ [ML^{-3}] is the density difference over the salt intrusion length, and υ [LT^{-1}] is the tidal velocity amplitude. The difference between N and N_r lies in the densimetric Froude number F_d [–] which is expressed as:

$$F_d = \frac{\rho}{\Delta\rho}\cdot\frac{\upsilon^2}{gh} \qquad 2.13$$

Since then, researchers have tried to look for a relation between dispersion and estuarine numbers. Laboratory results of WES flume (Van Rees and Rigter, 1969; Rigter, 1973),

Delft flume (Ippen and Harleman, 1961, 1967) and Daniels (1974) indicated an agreement with the result of Fischer (1972) in computing the salt intrusion length, using shear velocity instead of mean velocity in the estuarine Richardson number. Subsequently, the relationship between the dispersion and modified N_r also gave good correlation for all the other cases (mostly flume experiments). Thatcher and Harleman (1972) suggested that the longitudinal dispersion is proportional to the salinity gradient and included this in his one dimensional analytical salt intrusion model, which later was used by Fischer (1972) to model the vertical salinity and velocity distribution. A disadvantage of all these methods was that they did not account for convergence (implicitly assuming an infinitely large convergence length) and that the tidal excursion, as the most important mixing length scale, was missing in the derivations.

Deriving the dimensionless dispersion coefficient from scaling the steady-state salt balance equation, Savenije (2005) developed the following empirical predictive relation for the longitudinal dispersion at the estuary mouth for high water slack (HWS):

$$D_0^{HWS} = 1400 \frac{\bar{h}}{a} N_r^{0.5} (\upsilon E) \qquad 2.14$$

The estuary shape was represented by the ratio of the averaged depth h [L] to the convergence length a, while the dispersion was made dimensionless by the tidal velocity amplitude and tidal excursion which was not considered in any of the earlier studies. The applicability of these predictive equations have been widely tested in many estuaries including multi-channel estuaries.

Kuijper and van Rijn (2011) later modified the empirical equation using salinity measurements from 13 estuaries, in which they introduced the inclusion of the dimensionless friction (C^2/g). The predictive equation was divided into two depending on the types of channel – prismatic and convergent:

Convergence channel:

$$D_0 = 60 \alpha_c \sqrt{\pi} \left(\frac{\sqrt{\Delta \rho g h_0 / \rho}}{\upsilon} \right) \left(\frac{C^2}{g} \right) \left(\frac{|u|}{\upsilon} \right)^{0.5} \frac{E}{a} \upsilon h_0 \qquad 2.15$$

Prismatic channel:

$$D_0 = 60\alpha_c\sqrt{\pi}\left(\frac{\sqrt{\Delta\rho g h_0/\rho}}{\upsilon}\right)\left(\frac{C^2}{g}\right)\left(\frac{|u|}{\upsilon}\right)^{0.5}\upsilon h_0 \qquad 2.16$$

where u [LT^{-1}] is the fresh water velocity. These equations can be used to calculate dispersion locally at any location. The coefficient α_c is an additional calibration coefficient with the range of 0.7 to 1.3. From the result of Kuijper and van Rijn (2011), it is observed that the α_c coefficients for prismatic channels have values that are closer to 1.0, whereas for convergent channels, the coefficients are scattered within the range.

2.4 Salt Intrusion Length

Several researchers have tried to develop a general relation for the salt intrusion length. The development of such predictive equations was done empirically based on a reasonable amount of data. A pioneer effort was made by van der Burgh (1972), making use of prototype information from the Dutch and German estuaries. His equation for the salt intrusion length as summarized by Savenije (1992, 1993b, 2005) is as follows:

$$L^{TA} = 26\pi\frac{h_0}{K}F^{-1.0}N^{-0.5} \qquad 2.17$$

with,

$$F = \frac{\upsilon}{\sqrt{g h_0}} \qquad 2.18$$

and,

$$N = \frac{|Q_f|T}{P_t} = \frac{A|u|T}{A\upsilon T}\cdot\pi = \frac{|u|}{\upsilon}\cdot\pi \qquad 2.19$$

In this equation, L^{TA} [L] is the salt intrusion length at TA situation, F [–] is the Froude number, and P_t [L^3] is the tidal flood volume. Fischer (1974) re-analysed the data by Rigter (1973) and included the Darcy–Weisbach roughness and the densimetric Froude number, resulting in:

$$L^{LWS} = 17.7\frac{h_0}{f_D^{0.625}}F_d^{-0.75}N^{-0.25} \qquad 2.20$$

where LWS denotes low water slack. It is important to note here that Van der Burgh's coefficient K is replaced by the Darcy–Weisbach roughness $f_D = 8g/C^2$ [–] and F is represented by the densimetric Froude number F_d [–].

About 20 years later, Van Os and Abraham (1990) established a similar equation with a slightly different coefficient:

$$L^{LWS} = 4.4 \frac{h_0}{f_D} F_d^{-1} N^{-1} \qquad 2.21$$

All these methods were based on flume data with prismatic geometry. Savenije (1993b, 2005, 2012) who explicitly accounted for channel convergence and the tidal excursion, developed a predictive equation for the salt intrusion length at HWS. The reasoning was that the maximum salt intrusion length occurs during HWS, which is most important for water resources management. Based on Equation (2.14), the equation reads as:

$$L^{LWS} = a \ln\left(1400 \frac{\bar{h} E_0 v_0}{K a^2 u_0} N_r^{0.5} + 1\right) \qquad 2.22$$

where v_0 [LT^{-1}] is the tidal velocity amplitude at the mouth. It is worth noting that Savenije follows Van der Burgh's equation, with an additional shape indicator referring to the area convergence length a.

Most of the empirical equations discussed above are based on LWS except for Van der Burgh's and Savenije's methods which are based on TA and HWS, respectively. However, they can easily be brought in agreement with each other by adding $E/2$ or E to L^{HWS}, respectively. Here, we aim to develop a universal predictive equation for estimating the Van der Burgh and dispersion coefficient for TA condition, which can be applied in the salt intrusion model to predict the salinity profile for any estuary worldwide under different tidal and flood events.

CHAPTER 3

METHODOLOGY

3.1 Introduction

In this study, the main focus is on the gravitational mixing mechanism which leads to longitudinal dispersion in estuaries: the tide and density-driven dispersion. The predictive salt intrusion parameters are developed based on measurable data of geometry, fresh water discharge and tide. In total of 89 measurements data of 30 estuaries worldwide were used to develop the predictive equations. Measurements data from 7 newly surveyed estuaries were collected from 2011 to 2013 in Malaysia, whereas the remaining were compiled by revisiting the existing data available in the database of Savenije (2005) and from engineering reports. The locations of the estuaries studied are displayed in Figure (3.1).

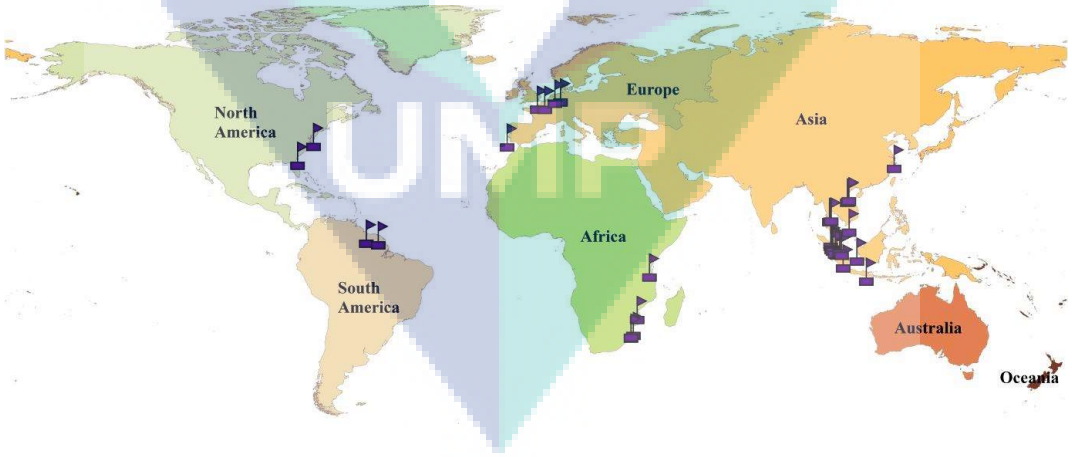

Figure 3.1 Global map showing the locations of estuaries studied.

Adjustment was made on the geometry and salinity analysis for some of the estuaries to ensure consistency in the input data used. The entire data were categorized into two

datasets: reliable and unreliable data. The reliable dataset are used to develop the predictive equations, whereas the unreliable ones were included only for observation purpose. This study was carried out based on Savenije's (1993b, 2005, 2012) method in predicting the equation for K and D with some modifications. The modifications made include:

1. All geometry and tide information used referred to the inflection point x1 as the boundary condition.
2. Analyses were carried out in TA condition instead of HWS, which is consistence with the geometry information.
3. Chezy roughness and estuary width to river width ratio are added into the predictive equations.
4. The parameters chosen are mostly independent and easy to measure without the need of prior calibration.

Although the predictive equations are based on the tidal average TA situation, one can still compute the salinity distribution for both low water slack LWS and high water slack HWS condition as they are mathematically related.

3.2 Selecting Dimensionless Ratios

Revising the parameters selected by Savenije (1993b, 2005), we found that the latter has some parameters that required tidal dynamics analysis priori and one of the ratio is not dimensionless. Considering the simplicity, we decided to reuse the dimensionless ratios of Savenije (1993b) including the dimensionless ratio for tidal effect from the recent equation. Since we know that the Van der Burgh's coefficient is not time dependent and is strongly related to geometry, the convergence length a or b and the width B of the estuary must be included. The followings are the dimensionless ratios selected for the equation to predict the Van der Burgh's coefficient:

$$K = f\left(\frac{B_f}{B_1}, \frac{g}{C^2}, \frac{E_1}{H_1}, \frac{h_1}{a_2}, \frac{h_1}{H_1}, \frac{\lambda_1}{E_1}\right) \qquad 3.1$$

where B_f [L] is the river regime width (located upstream of the tidal limit where the convergence of the river width is modest and near constant), and $\lambda_1 = T\sqrt{g\bar{h}_1/r_s}$ [L] is the wave length at the inflection point with r_s [–] being the storage width ratio (defined as the ratio between storage width and stream width). The symbols B_1 [L], E_1 [L], h_1 [L], H_1 [L] and b_2 [L] represent the estuary width, tidal excursion, averaged estuary depth, tidal range and width convergence length at the inflection point x_1. It is worth noting that the roughness $C = K_m \bar{h}_1^{1/6}$ was obtained through calibration using the tidal dynamics solution of Cai et al. (2012) which makes use of observed tidal damping. In the above equation, it can be seen that all the parameters used have a boundary condition at the inflection point x_1. It is also worth noting that the convergence length adopted is of the second reach not the first part of the estuary. For the tidal indicators such as E and H, the measurements were always taken at the mouth. In order to obtain the tidal excursion and tidal damping at the inflection point, a projection can be made with tidal damping as follows (Kuijper and Van Rijn, 2011):

$$H_1 = H_0 \cdot e^{\delta x_1} \qquad 3.2$$

$$E_1 = E_0 \cdot e^{\delta x_1} \qquad 3.3$$

where the damping factor δ_H also follows from the tidal dynamics simulation of Cai et al. (2012). The values of H_1 and E_1 used in the dimensionless ratios represent the condition of spring tide, where v is considered to be close to 1 ms^{-1} (Bruun and Gerritsen, 1960; Pethick, 1984; Langbein, 1963). This is to ensure that K is time independent representing a general characteristic of an estuary. As a result, E essentially reflects the tidal period as described in (see also Table 3.1).

$$E = \frac{vT}{\pi} \qquad 3.4$$

For the dispersion coefficient, eight dimensionless ratios were selected, and 18 combinations including the one of Savenije (1993b, 2005) were established and tested. The dispersion coefficient is also represented in dimensionless form as:

$$\frac{D_1}{\upsilon_1 E_1} = f\left(N_{r1}, \frac{h_1}{a_2}, \frac{g}{C^2}, \frac{H_1}{E_1}, \frac{h_1}{E_1}, \frac{\lambda_1}{E_1}, \frac{\lambda_1}{a_2}, \frac{B_1}{h_1}\right) \quad 3.5$$

with,

$$N_{r1} = \frac{\Delta\rho}{\rho}\frac{g h_1}{\upsilon_1^2}\frac{Q_f T}{A_1 E_1} \quad 3.6$$

where N_{r1} [–] is the estuarine Richardson number with υ_1 [LT^{-1}] being the tidal velocity amplitude, both at the inflection point. It is important to note that the values taken for E_1 and H_1 in the dispersion analysis are based on the real-time data captured during measurements and the depth is referring to the depth at the inflection point.

In general, the density different between the saline and fresh water is taken as 25 kg/m3 and fresh water density as 1000 kg/m3. The fresh water discharge data were adjusted for the 7 newly surveyed estuaries so that the runoff contributed by the downstream sloped area of the gauged catchment is also considered in the analysis. Stepwise multiple regression analysis is applied to identify the best combination of the dimensionless ratios in predicting the Van der Burgh's and dispersion coefficient. The efficiency of the established equations was examined by comparing the correlation coefficient R2 and the standard error SE. The predicted results calculated by the most suitable equations were plotted against the calibrated values to evaluate their predictive performance.

3.3 Substitution of Predictive Equations In Salt intrusion Model

In the sense that the dispersion coefficient prediction computed is at the inflection point x_1, reverse calculation to obtain the dispersion at the mouth has to be done. This is essential to enable the simulation of the longitudinal salinity distribution starting from the mouth to the salt intrusion limit. The dispersion at the estuary can be computed by:

$$D_0^{TA} = D_1^{TA}\left\{1 + \beta_{rev}^{TA}\left[e^{\left(\frac{x_1}{a_1}\right)} - 1\right]\right\} \quad 3.7$$

with,

$$\beta_{rev}^{TA} = \frac{K a_1}{\alpha_1^{TA} A_0} \quad 3.8$$

and,

$$\alpha_1^{TA} = \frac{Q_f}{D_1^{TA}} \tag{3.9}$$

where β_{rev} [–] is the reversed dispersion reduction rate, whereas A_1 [L^2], D_1 [L^2T^{-1}] and α_1 [L^{-1}] are the cross-sectional area, dispersion coefficient and mixing number at the inflection point, respectively. It is important to note that the convergence length a_1 [L] applied in Equations (3.7) and (3.8) is of the first section of the estuary. The relation between dispersion and salinity is then expressed by:

$$\frac{S^{TA} - S_f}{S_0^{TA} - S_f} = \left(\frac{D^{TA}}{D_0^{TA}} \right)^{1/K} \quad \text{for } 0 < x \leq x_1 \tag{3.10}$$

$$\frac{S^{TA} - S_f}{S_1^{TA} - S_f} = \left(\frac{D^{TA}}{D_1^{TA}} \right)^{1/K} \quad \text{for } x > x_1 \tag{3.11}$$

where S_0 [ML^{-3}] and S_1 [ML^{-3}] refer to the salinity at the estuary mouth and the inflection point, respectively.

At the first reach where x < x1, the salt intrusion curve has a dome shape, whereas after the inflection point, the curve turns to a recession shape. Substituting the tidally average dispersion coefficient into the general form of the salt intrusion length of Savenije (1993b, 2005) yields:

$$L^{TA} = x_1 + a_2 \ln\left(\frac{1}{\beta_1^{TA}} + 1 \right) \tag{3.12}$$

with,

$$\beta_1^{TA} = \frac{K a_2}{\alpha_1^{TA} A_1} \tag{3.13}$$

Note that all parameters used in these equations refer to the inflection point. We obtain the salinity profile at HWS and LWS by moving the salinity curve over $E/2$ in the upstream and downstream direction. Similarly, the maximum salt intrusion length can be

obtained by shifting the intrusion length at TA in the landward direction by half of the tidal excursion at the mouth as:

$$\beta_1^{TA} = \frac{Ka_2}{\alpha_1^{TA} A_1} \tag{3.14}$$

Shifting the intrusion length at TA by half of the tidal excursion seaward gives the minimum salt intrusion length.

$$L^{LWS} = L^{TA} - \frac{E_0}{2} \tag{3.15}$$

Table 3.1 Data used to develop the predictive equation for the coefficient K

No	Estuary	A_1 [10^3] (m^2)	a_2 (km)	B_1 (m)	B_f (m)	b_2 (km)	$\bar{h}_1$ (m)	x_1 (km)	H_0 (m)	E_0 (km)	T (h)	K_m	δ_H (10^{-6} m^{-1})	K Cal	K Pre
Reliable sets for calibration															
1	Kurau	0.7	46	130	20	28	6.2	3.6	2.3	14	12	30	−6.30	0.40	0.35
2	Perak	9.2	37	2070	130	21	6.3	4.0	2.8	14	12	65	3.00	0.20	0.24
3	Bernam	4.5	25	1270	45	17	5.3	4.3	2.9	14	12	70	1.70	0.20	0.22
4	Selangor	1.0	13	270	35	13	3.7	2.8	4.0	14	12	40	−3.70	0.34	0.42
5	Muar	1.6	100	280	55	31	8.2	3.9	2.0	14	12	45	−2.68	0.25	0.32
6	Endau	2.0	44	310	72	44	6.5	4.8	1.9	14	12	45	−1.30	0.40	0.33
7	Maputo	4.7	16	1150	100	16	4.1	5.1	3.3	14	12	58	2.00	0.38	0.32
8	Thames	10.9	23	780	50	40	8.2	31.0	5.3	14	12	45	1.10	0.20	0.24
9	Corantijn	26.8	64	5000	400	48	6.7	18.0	3.1	14	12	40	−1.70	0.21	0.27
10	Sinnamary	1.1	39	470	95	12	3.9	2.7	3.3	14	12	40	−5.00	0.45	0.46
11	MaeKlong	1.1	150	240	150	150	4.6	3.2	3.6	14	12	40	−4.20	0.30	0.48
12	Lalang	2.9	167	360	130	94	10.3	0.0	2.6	28	24	84	−0.54	0.65	0.57
13	Limpopo	1.1	115	180	90	115	6.3	20.0	1.9	14	12	43	1.70	0.50	0.38
14	Tha Chin	1.4	87	260	45	87	5.6	5.0	2.6	14	12	50	−5.50	0.35	0.31
15	ChaoPhya	3.1	130	470	200	130	6.5	12.0	3.4	28	24	65	−2.20	0.75	0.71
16	Edisto	5.2	15	1250	60	15	4.1	2.0	3.2	14	12	30	−8.80	0.35	0.31
17	Elbe_Flanders	27.3	70	3040	350	80	8.5	33.0	4.7	14	12	32	2.00	0.30	0.27
17a	Elbe_Kuijper	46.0	66	4500	350	66	10.2	0.0	4.7	14	12	32	2.00	0.30	0.25
17b	Elbe_Savenije	43.0	66	2880	350	50	11.7	0.0	4.6	14	12	32	2.00	0.30	0.28
18	Pangani	0.9	15	270	35	15	3.2	3.1	4.2	14	12	42	10.00	0.60	0.41
19	Linggi	1.5	8	320	25	13	3.2	0.5	2.0	14	12	30	−14.00	0.30	0.36
20	Landak	2.0	60	230	100	60	8.7	0.0	1.6	28	24	45	−6.70	0.60	0.69
Less reliable sets for verification															
21[3,4]	Delaware	255.0	41	37 655	120	42	6.4	0.0	1.8	14	12	55	0.65	0.22	0.09
22[2,3]	Westerschelde	150.0	27	16 000	50	27	9.4	0.0	4.0	14	12	46	2.80	0.25	0.10
23[1,2,4]	Pungue	14.5	19	5200	50	19	2.8	0.0	6.7	14	12	31	−8.50	0.30	0.22
24[2]	Incomati	1.1	40	380	22	40	2.8	15.0	3.3	14	12	56	−19.90	0.15	0.34
25[2,4]	Solo	2.1	226	225	95	226	9.2	0.0	1.8	28	24	31	3.00	0.60	0.64
26[2,4]	Eems	120.0	19	31 623	55	19	3.8	0.0	3.6	14	12	31	−0.70	0.30	0.11
27[2,3]	Tejo	100.0	13	20 000	180	13	5.0	0.0	3.6	14	12	56	2.20	0.90	0.16
28[2,4]	Rompin	0.8	110	140	50	110	6.1	19.0	2.5	14	12	15	−33.40	0.30	0.64
29[2,4]	Ulu Sedili Besar	0.7	38	140	35	49	4.1	4.3	2.5	14	12	30	−25.50	0.30	0.45
30[1,3]	Gambia	35.7	96	3700	110	100	8.8	33.0	1.83	14	12	35	−1.00	0.60	0.16

Note: [1] Non-steady state (NSS); [2] uncertain discharge (UQ); [3] non-alluvial (NA); [4] information lacking (IL).

3.4 Data

Data were divided into two categories: reliable and less reliable. There are 47 measurements grouped under the reliable data set, and 38 measurements under the less reliable data set. This distinction was made based on the following criteria.

Criteria for classifying estuaries as reliable:

- the estuary is generally in steady-state condition;
- the fresh water discharge is estimated, observed or measured correctly;
- the estuary is alluvial and undisturbed;
- complete measurement data for tidal dynamics and
- salinity analyses are available.

Criteria for classifying estuaries as less reliable:

- The estuary is not in steady state particularly during low river discharge. This depends on the ratio of the timescale of system response to the timescale of discharge reduction (see Savenije, 2012) (NSS).
- The estimation of the fresh water discharge is uncertain (UQ).
- The estuary may not be alluvial (e.g. dredged, modified or constricted by rocky banks) (NA).
- Information on tidal dynamics and salinity is lacking or unclear (IL).

The estuaries that fall under category NSS, UQ, NA and IL are listed in Table 3.1. It is worth noting that only the reliable set is used in regression analysis. The less reliable ones are merely plotted for verification purpose.

CHAPTER 4

RESULTS AND DISCUSSIONS

4.1 Predictive equation for the Vander Burgh's coefficient *K*

Results from the stepwise multiple regression analyses show that the best combinations of the dimensionless ratio to represent the Van der Burgh's predictive equation are:

$$K_a = 3.54\times10^{-3}\left(\frac{B_f}{B_1}\right)^{0.40}\left(\frac{g}{C^2}\right)^{0.05}\left(\frac{E_1}{H_1}\right)^{0.86}\left(\frac{h_1}{a_2}\right)^{0.24}\left(\frac{H_1}{h_1}\right)^{0.56}\left(\frac{\lambda_1}{E_1}\right)^{0.29} \quad 4.1$$

or,

$$K_a = 3.44\times10^{-3}\left(\frac{B_f^{0.40} g^{0.20} E_1^{0.57} T^{0.29}}{B_1^{0.40} C^{0.10} a_2^{0.24} h_1^{0.17} H_1^{0.30}}\right) \quad 4.2$$

where Equation (4.2) is the simplified form. In the case where the cross-sectional area information is not available, the convergence length a_2 can be replaced by the width convergence length b_2. The equation then becomes:

$$K_b = 1.83\times10^{-3}\left(\frac{B_f}{B_1}\right)^{0.38}\left(\frac{g}{C^2}\right)^{0.10}\left(\frac{E_1}{H_1}\right)^{0.98}\left(\frac{h_1}{b_2}\right)^{0.24}\left(\frac{H_1}{h_1}\right)^{0.60}\left(\frac{\lambda_1}{E_1}\right)^{0.28} \quad 4.3$$

$$K_b = 1.78\times10^{-3}\left(\frac{B_f^{0.38} g^{0.24} E_1^{0.70} T^{0.28}}{B_1^{0.38} C^{0.20} b_2^{0.24} h_1^{0.22} H_1^{0.38}}\right) \quad 4.4$$

The correlation coefficient R^2 and the standard error obtained for Equation (4.2) is 0.76 and 0.099, while for Equation (4.4) is 0.77 and 0.097, respectively. From both equations, we can see that the parameter that has the most influence on the Van der Burgh's

coefficient is the tidal excursion which has the power of 0.57 and 0.70. The estuary to river width ratio shows higher power than the convergence length, which indicates that the width is a better shape indicator. Figure (4.1) show plots of the predicted *K* against the calibrated one for both cases. All the reliable data points seem to fall close to the perfect agreement line. About half the unreliable data points were outliers particularly the Gambia and Tejo Estuary which is much further away from the perfect agreement line. This is not strange in the sense that the Tejo Estuary not entirely alluvial, and its narrow and deep mouth caused by a rock outcrop formation turns it into a fjord type estuary. As for Gambia, it is in unsteady state estuary. Nevertheless, for the rest of the outliers we believe that they will fit in better if good data is present.

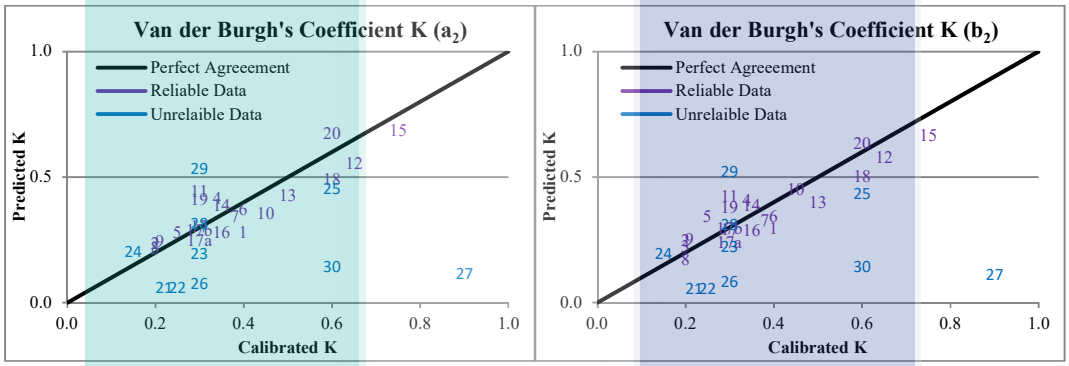

Figure 4.1 Performance of the predictive equation *K*

4.2 Predictive equation for the dispersion coefficient *D*

Since results of the predicted *K* using both convergence lengths are close, only the cross-sectional area convergence length is used in the analysis to develop the predictive equation for dispersion. In this study, 18 combinations of the dimensionless ratios were established with multiple regression method and the results are displayed in Table (4.1). Figure (4.2) shows the correlations and standard error for each of the predictive equations. It seems that except for Equations R1, R17 and R18, all the equations have reasonably high performance in predicting the dispersion coefficient.

If we only look at the performance chart, it is very hard to decide which equation is the best. However, from the equations, we can identify which parameters are more important by observing the exponent. It can be obviously seen that the variation of the

power value for the Estuarine Richardson number N_r is modest, and this means that the dispersion is strongly correlated with N_r compared to the other parameters. The reason Equation R2 to R16 have almost the same performance is because adding new dimensionless ratios to Equation R2 does not make any great changes. The only parameters that give higher exponent are the ratio of the gravity to Chezy roughness.

Table 4.1 Results obtained from the multiple regression analysis

Equations for multiple regression analysis			
$\frac{D_1^{TA}}{\upsilon_1 E_1} = 2141 N_r^{0.84} \left(\frac{h_1}{a_2}\right)$	(R1)	$\frac{D_1^{TA}}{\upsilon_1 E_1} = 0.2942 N_r^{0.56} \left(\frac{a_2}{h_1}\right)^{0.04} \left(\frac{g}{C^2}\right)^{0.23}$	(R10)
$\frac{D_1^{TA}}{\upsilon_1 E_1} = 0.1167 N_r^{0.57}$	(R2)	$\frac{D_1^{TA}}{\upsilon_1 E_1} = 0.1400 N_r^{0.57} \left(\frac{g}{C^2}\right)^{0.27} \left(\frac{E_1}{H_1}\right)^{0.16}$	(R11)
$\frac{D_1^{TA}}{\upsilon_1 E_1} = 0.1515 N_r^{0.58} \left(\frac{h_1}{a_2}\right)^{0.03}$	(R3)	$\frac{D_1^{TA}}{\upsilon_1 E_1} = 0.4225 N_r^{0.57} \left(\frac{g}{C^2}\right)^{0.22} \left(\frac{a_2}{\lambda_1}\right)^{0.02}$	(R12)
$\frac{D_1^{TA}}{\upsilon_1 E_1} = 0.3958 N_r^{0.57} \left(\frac{g}{C^2}\right)^{0.21}$	(R4)	$\frac{D_1^{TA}}{\upsilon_1 E_1} = 0.3873 N_r^{0.57} \left(\frac{g}{C^2}\right)^{0.21} \left(\frac{\lambda_1}{E_1}\right)^{0.01}$	(R13)
$\frac{D_1^{TA}}{\upsilon_1 E_1} = 0.1812 N_r^{0.57} \left(\frac{H_1}{E_1}\right)^{0.05}$	(R5)	$\frac{D_1^{TA}}{\upsilon_1 E_1} = 39.7568 \left(N_r \cdot \frac{g}{C^2} \cdot \frac{H_1}{E_1}\right)^{0.43}$	(R14)
$\frac{D_1^{TA}}{\upsilon_1 E_1} = 0.1344 N_r^{0.57} \left(\frac{h_1}{E_1}\right)^{0.02}$	(R6)	$\frac{D_1^{TA}}{\upsilon_1 E_1} = 0.2708 \left(N_r \cdot \frac{g}{C^2} \cdot \frac{\lambda_1}{E_1}\right)^{0.45}$	(R15)
$\frac{D_1^{TA}}{\upsilon_1 E_1} = 0.1243 N_r^{0.58} \left(\frac{E_1}{\lambda_1}\right)^{0.02}$	(R7)	$\frac{D_1^{TA}}{\upsilon_1 E_1} = 0.1400 N_r^{0.57} \left(\frac{a_2}{h_1}\right)^{0.002} \left(\frac{g}{C^2}\right)^{0.27} \left(\frac{E_1}{H_1}\right)^{0.16}$	(R16)
$\frac{D_1^{TA}}{\upsilon_1 E_1} = 0.1138 N_r^{0.58} \left(\frac{\lambda_1}{a_2}\right)^{0.02}$	(R8)	$\frac{D_1^{TA}}{\upsilon_1 E_1} = 0.0928 \left(\frac{g}{C^2}\right)^{0.26} \left(\frac{E_1}{H_1}\right)^{0.02}$	(R17)
$\frac{D_1^{TA}}{\upsilon_1 E_1} = 1.9474 \left(N_r \cdot \frac{g}{C^2}\right)^{0.51}$	(R9)	$\frac{D_1}{\upsilon_1 E_1} = 0.5746 \left(\frac{g}{C^2}\right)^{0.31} \left(\frac{h_1}{B_1}\right)^{0.27}$	(R18)

It is also interesting to note that the performance of the selected dimensionless ratios based on Savenije (199b, 2005) equation (here R1) is rather poor. Furthermore, the exponent obtained for N_r is also higher than the one in the existing equation. These significant different may be caused by the changes made in some of the input information (e.g. geometry), and the used of the selective data for calibration. From the comparisons,

we concluded that Equation R4 is the best in predicting the dispersion coefficient. Nevertheless, if the Chezy roughness is unknown, then Equation R2 can be applied.

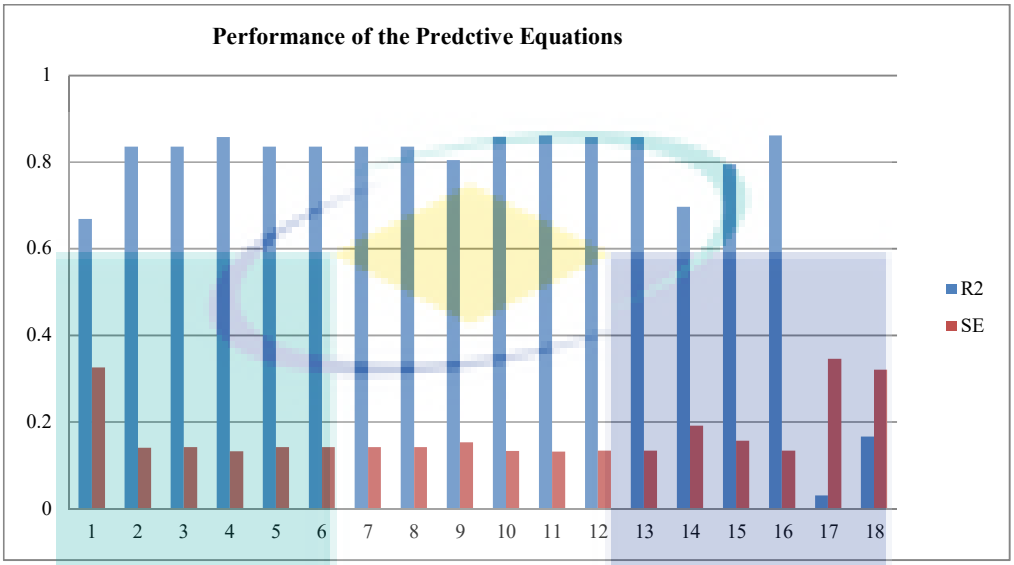

Figure 4.2 Performance of the predictive equations obtained from theregression analysis.

Figure (4.3) displayed the plots of the predicted D_1 and α_1 against the calibrated values for both the reliable and unreliable datasets using Equation R1, R2, R4 and R9. From the plot, it shows that the D and α plot using Equation R1 display a highly scattered pattern for both the reliable and unreliable datasets. For Equation R2, R4 and R9, all the reliable data points fall nicely within the range of factor 1/1.5 to 1.5. Some of the unreliable data points are also within or near the range except several obvious outliers such as the Delaware, Schelde, Pungue, and Tejo. This is because for the Pungue, the ratio of h/H is smaller than unity which makes it in an unsteady state condition. Schelde is a navigated estuary and Delaware has very high discharge. Moreover, the doubt on the accuracy of the data is also one of the factor contributing to poor results. It can be seen that all the predictive equations selected have underestimated the values of the dispersion coefficient for the outlying data points.

Comparing the outliers in both plots, it seems that the unreliable data are distributed closer to the reference lines if the dispersion is represented in term of α. This means that the fresh water discharge is indeed has a role in the mixing mechanism. Furthermore, it shows the underestimation of the unreliable data points is partly caused

by incorrect streamflow data. Nevertheless, the tidal dynamics and geometry characteristics are believed to be the main factors causing the significant outlier.

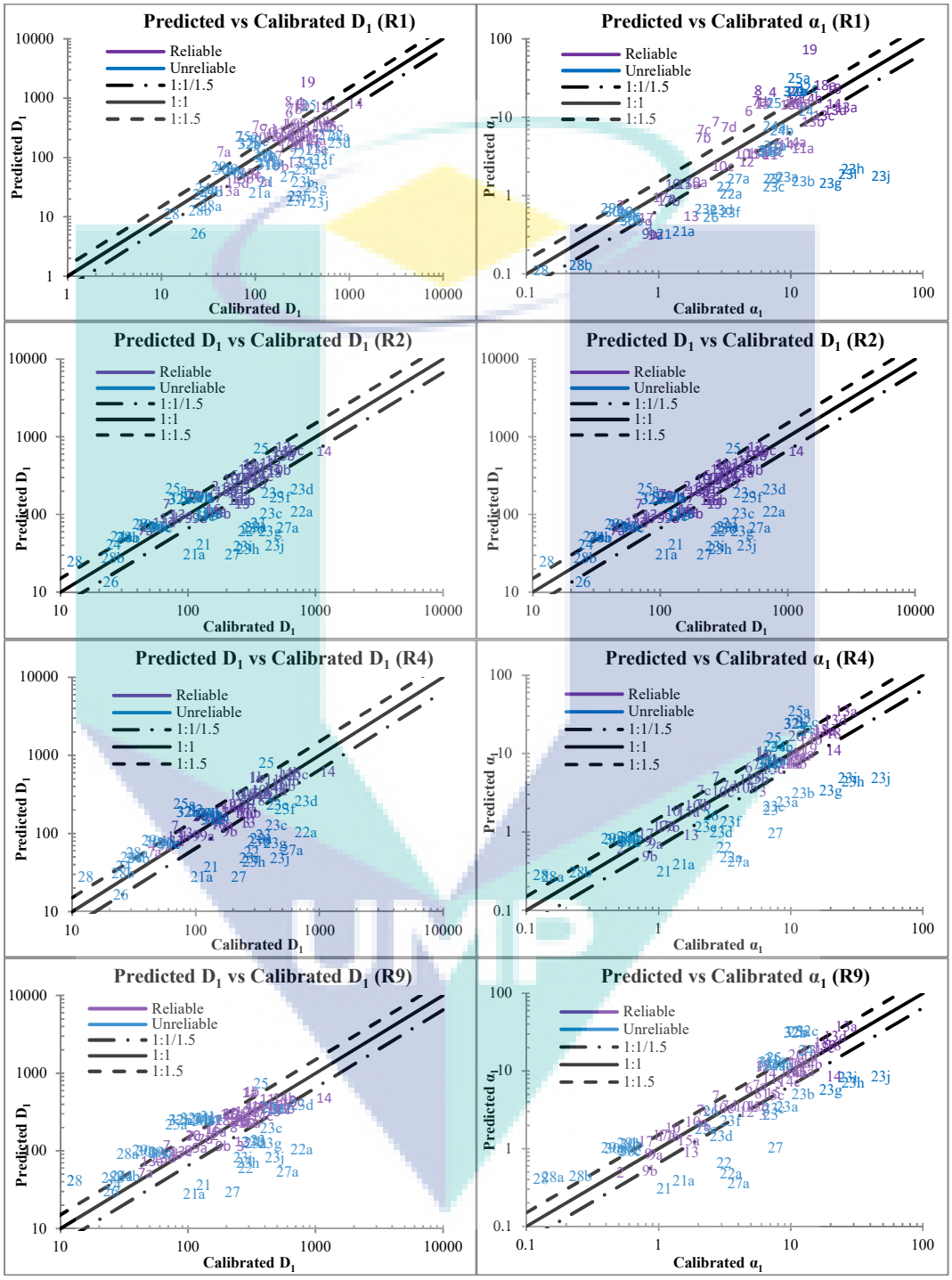

Figure 4.3 Performance of the predictive equations for the dispersion coefficient (left panel) and mixing number (right panel) against calibrated values.

4.3 Modified Predictive Equation for Maximum Salt Intrusion Length L^{HWS}

Comparison between the predicted and calibrated salt intrusion length has been done for HWS condition instead of TA. This is because the salt intruded furthest into the river system at HWS, and the maximum intrusion is the information water managers most interested in. Substituting the predictive dispersion equations established into the general form of salt intrusion length equation yields:

$$L^{HWS} = x_1 + a_1 \ln\left(2141\frac{h_1 E_1 \upsilon_1}{K_a a_2^2 u_1} N_r^{0.84} + 1\right) + \frac{E_0}{2} \quad 4.5$$

$$L^{HWS} = x_1 + a_1 \ln\left(0.1167\frac{E_1 \upsilon_1}{K_a a_2 u_1} N_r^{0.57} + 1\right) + \frac{E_0}{2} \quad 4.6$$

$$L^{HWS} = x_1 + a_1 \ln\left(0.3958\frac{E_1 \upsilon_1 g^{0.21}}{K_a a_2 u_1 C^{0.42}} N_r^{0.57} + 1\right) + \frac{E_0}{2} \quad 4.7$$

$$L^{HWS} = x_1 + a_1 \ln\left(1.9474\frac{E_1 \upsilon_1 g^{0.51}}{K_a a_2 u_1 C^{1.02}} N_r^{0.51} + 1\right) + \frac{E_0}{2} \quad 4.8$$

Figure (4.4) shows the performance of the equations in predicting the maximum salt intrusion length. From the plots, all the data points fall within the range of factor 1.5 except of the Solo Estuary. This confirmed that adding the shape factor in the equation is indeed essential in determining the salt intrusion length as claimed by Savenije (1993b). It seems that the predictive equations overestimated the intrusion length in Solo Estuary. It may be due to the nearly prismatic shape of the channel which has a very long convergence length of 226 km.

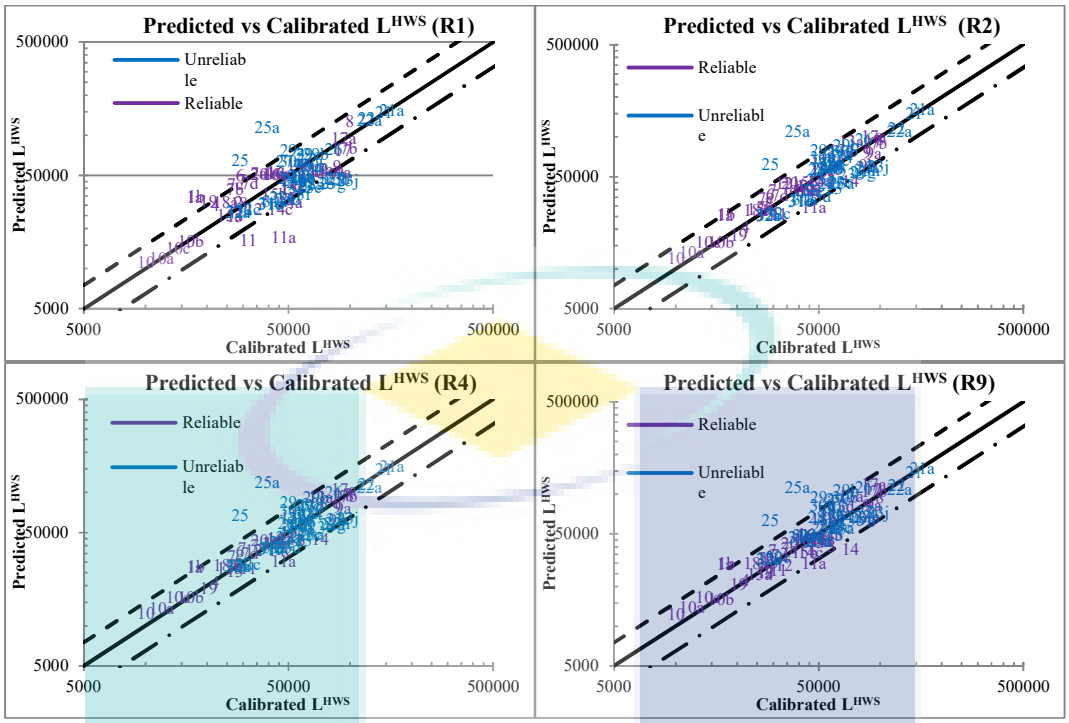

Figure 4.4 The performance of the equations in predicting the maximum salt intrusion length.

4.4 Longitudinal Salinity Profiles

Performing the backward calculation using the dispersion predictive equations, we are able to compute the dispersion at the mouth D_0 of the estuary. Subsequently, salinity curve can be simulated by applying Equations (3.10) and (3.11) with the different dispersions calculated by each of the predictive measure developed. Considering the substantial amount of salinity measurements available, only the salinity profiles of the 7 newly surveyed estuaries are discussed. The plots for the entire salinity profiles are provided in the supporting documents. Figure (4.5) demonstrate the performance of the simulated longitudinal salinity distribution with and without calibration of K and D.

It can be seen from Figure (4.5) that except for R1, all the predicted D and K applied in the salt model provide good simulated results near the estuary mouth in reference to the calibrated ones. However, the fully predictive salinity curves tend to divert further from the calibrated curves somewhere after the inflection point. This can be explained by two possibilities: the Van der Burgh's coefficient K and effect from the

fresh water discharge Q_f. From the shape analysis, we know that the shape factor K has most influence at the tail of the salinity curves. Since the R2 correlation for the Van der Burgh's predictive equation is about 0.76, the error from the regression may contributes to the diversion of the curve. In chapter 2, it is known that the beginning from the middle reach to the end of the salt intrusion region, the dominated mixing mechanism gradually moving from tide to density driven dispersion. Hence, this once again confirmed the influence of fresh water discharge to the salt intrusion process particularly at the upstream part.

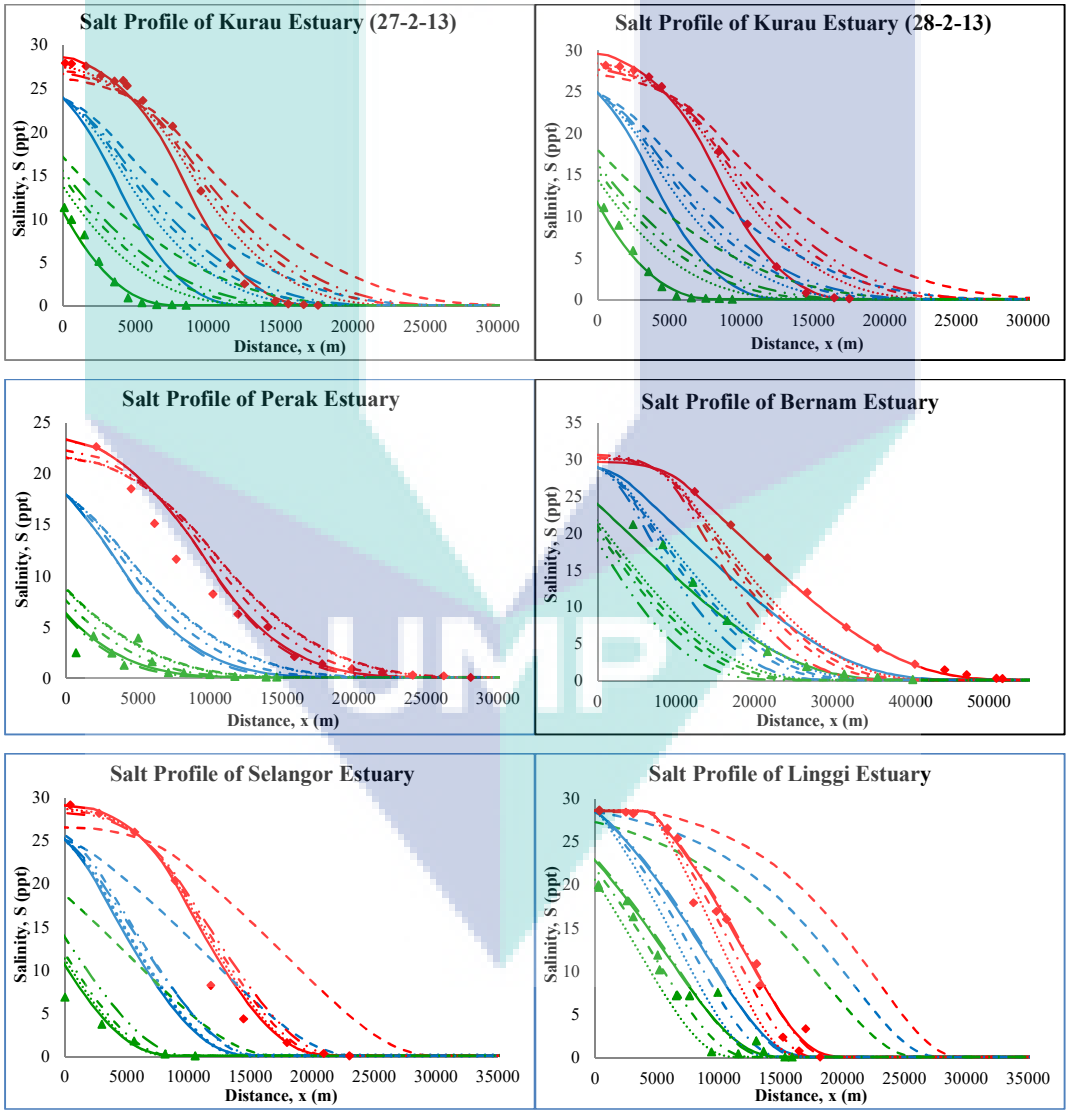

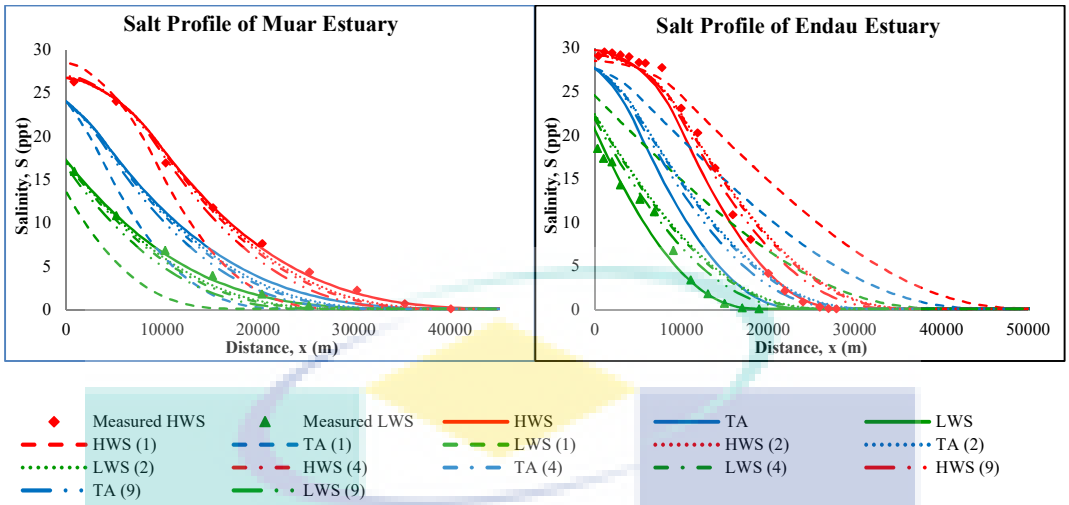

Figure 4.5 Calibrated (solid lines) and predicted (dashed lines) salinity curves compared to observations (symbols) for HWS, TA and LWS in the seven newly surveyed Malaysian estuaries.

It is interesting to note that Equation R9 works better in predicting the salinity distribution for some of the estuaries such as the Perak, Linggi and Endau estuary. As for most of the cases, Equation R2 seems to give the best fitting. The inconsistency in the performance of the equations suggests that there is a possibility that better conclusion can be made in selecting the best combinations if more reliable measurements data are available. Thus, it is appropriate to retain all the three equations (R2, R4 and R9) into consideration.

4.5 Discussion

Before Savenije's (1993a) effort to develop the predictive equations for Van der Burgh's and dispersion coefficient, these parameters can only be obtained by calibration. Without site measurements data, it is impossible to have any estimation of the salinity distribution along an estuary in priori. The predictive measures of Savenije (1993a, 2005) are able to estimate the value of K and D reasonably well in reference to the calibrated result. However, after the re-evaluating and re-analysing the available data, we found that the equations do not work well for some of the estuaries.

In this study, we have collected an additional of 32 measurements from 16 estuaries to consider in the analysis. Moreover, the measurements were sectioned into

two datasets to make sure that only the reliable data are used for developing the equations. In the previous work, the data are not separated. The selection process is important so that the results are not influenced by the incomplete or uncertain data. Re-examining the available measurements from the old database (not properly compiled) ensures that all the data used are accessible and consistent. The new compilation also provides a section to note important information about each measurement.

Another important modification in this work is the change in the boundary condition chosen. From the existing research discussed in the earlier section, we understand the cross-sectional data were processed in reference to the tidal averaged level (TA). However, except Van der Burgh (1972) and Savenije (1989), Rigter (1973), Fischer (1974), and Van Os and Abraham (1990) introduced the empirical salt intrusion length equations for LWS condition. The inconsistency may create uncertainty since the geometry during low water can be quite different from tidal average situation. Savenije later changed his salt intrusion model from the reference of TA (1989) to HWS (1993a) condition. For the purpose to standardize application of the data in the analyses, we decided to set the reference at TA condition.

The downstream boundary set in this study is located at the inflection point x1 not the estuary mouth (adopted by all the earlier researchers). The reasons and advantages of moving the downstream boundary slightly inland are:

1. to eliminate the difficulty of determining the exact location of the estuary mouth.
2. to reduce the effect from the wind and wave.
3. to reduce the possibility of over-mixing or throttling near the mouth.
4. the dominated area is more stable (in steady state condition), and generally water extraction pumping stations are situated in this region.
5. to eliminate the dilemma of which geometry parameters to use particularly when converting the salt intrusion distribution from TA to HWS condition: first reach near the mouth or second reach after the inflection point.

In Savenije (1993a, 2005) and Kuiper and van Rijn's (2011) predictive model, the cross-sectional area convergence length applied to calculate the salt intrusion length is the weighted value obtained from an iteration process. Hence, with the change of the downstream boundary to x_1, this process no longer needed and the predictive measures can be more accurate.

The new set of dimensionless ratios proposed in this study to establish the predictive equation for K contains mostly measurable independent parameters. Selection was made based on the existing equations, considering only the parameters that is easy to get. It is worth noting that the ratio $(1-\delta_H b)$ is removed in the equation because the damping always changes from spring to neap tide. Furthermore, it also decreases or decreases towards upstream and is highly influenced by fresh water discharge. The river to estuary width ratio is added in the new equation as an additional geometry indicator besides the depth and convergence length.

For the predictive dispersion equation, the ratio of the depth to the convergence length is no longer valid, but the longitudinal length scale and velocity υE is still maintained. The elimination of h/a allows the new equation to be applied also in prismatic channel. In the existing equation, when a_2 is near to infinity, the calculation becomes invalid. Since Kuijpers and van Rijn (2011) suggested that friction parameter is related to the vertical mixing, g/C^2 is included in this new equation and it indeed improves the correlation. Savenije (2005) did not consider roughness in his predictive equation for dispersion.

Although some improvements and simplicity have been introduced in this study, there are limitations in using the new equations. In the meantime, we only take into account single network estuaries in our datasets. Furthermore, it is assumed that no is water coming in and going into the tributaries in the estuary region. The applicability of the predictive measures in multi-channel estuaries and for those with huge tributaries is still unknown. From the plot of Van der Burgh's coefficient, we found that the performance in predicting the shape factor is rather poor. This indicates that the equation has to be used cautiously in estuary which is in unsteady state condition. The ratio h/a in the Van der Burgh predictive equation restricts its application in prismatic channel. Another constraint in using the developed equations is the friction factor. The Chezy roughness is not measurable and can only be obtained by calibration from the tidal

dynamics analysis (Cai et. al. 2012). However, if this information is impossible to get, it can be neglected (e.g. the correlation only decrease to 0.75 for the *K* predictive equation).

It is recommended to collect more reliable measurements to strengthen the development of the empirical relationships. New data is also required for validation purpose. If new data is not possible, validation may be carried out using virtual data and compare the results with other the method such as numerical model.

CHAPTER 5

CONCLUSION AND RECOMMENDATIONS

5.1 Introduction

Calibrating the van der burgh's and dispersion coefficient is only possible if measurements data of salinity distribution are available. In a situation where data are limited, a predictive equation can be very useful to estimate the desired variable. A good predictive equation must be simple (parameters can be easily measured) and efficient. The predictive equations established in this study consist of mostly measurable independent parameters. Options are suggested for the case in which data are very limited. The adjustment of the downstream boundary to the inflection point has prevent the dilemma of selecting the right geometry parameters to use. Analysis based on tidal average condition enable the entire process to be carried out in consistency, and possible model and data error can be reduced. The results for dispersion and salt intrusion length can easily converted from TA to HWS by adding half of the tidal excursion. However, one must make sure that the conversion for the dispersion must be made at the inflection before performing backward calculation to obtain the HWS dispersion at the mouth. The performance of the predictive equation for K is rather good with a R2 value of 0.76. For the dispersion, the correlation of 0.85 seems very promising. All the reliable data points fall within the factor 1.5 for both the predicted K and D results. Some unreliable ones are also in the range. This indicates that the predictive equations developed is appropriate to be applied in getting a first estimate on the K and D. Subsequently, the longitudinal salinity distribution in an estuary can be simulated. Hence, these tools can be very helpful for water manager and engineering to carry out preliminary estimated on the salt intrusion condition in the estuary of interest.

REFERENCES

Bruun, P. and Gerritsen, F.: Stability of Coastal Inlets, North Holland Pub. Co., Amsterdam, 128 pp., 1960.

Cai, H., Savenije, H. H. G., and Toffolon, M.: A new analytical framework for assessing the effect of sea-level rise and dredging on tidal damping in estuaries, J. Geophys. Res.-Oceans, 117, C09023, doi:10.1029/2012JC008000, 2012.

Daniels, D. G.: A Laboratory Study of Estuarine Salinity Intrusion in a Rectangular Channel of Large Aspect Ratio, Hydraul. Eng. Lab. Rep. WHM-17, Univ. Calif., Berkeley, 65 pp., 1974.

Fischer, H. B.: Mass transport mechanisms in partially stratified estuaries, J. Fluid Mech., 53, 671–687, 1972.

Fischer, H. B.: Discussion of "Minimum Length of Salt Intrusion in Estuaries" by Ben P. Rigter, J. Hydr. Eng. Div.-ASCE, 100, 708–713, 1974.

Fischer, H. B.: Mixing and dispersion in estuaries, Ann. Rev. Fluid Mech., 8, 107–133, 1976.

Gisen, J. I. A. and Savenije, H. H. G.: Estimating bankfull discharge and depth in ungauged estuaries, Water Resour. Res., 51, 2298 – 2316, 2015.

Gisen, J. I. A., Savenije, H. H. G., Nijzink, R. C., and Abd. Wahab, A. K.: Testing a 1-D analytical salt intrusion model and its predictive equations in Malaysian stuaries, Hydrol. Sci. J., 60, 156–172, 2015.

Harleman, D. R. F. and Abraham, G.: One-Dimensional Analysis of Salinity Intrusion in the Rotterdam Waterway, Hydraulics Laboratory Publ. No. 44,Waterloopkundig Laboratorium, Delft, 1966.

Ippen, A. T. and Harleman, D. R. F.: One-dimensional analysis of salinity intrusion in estuaries, US Army Corps Eng., Waterways Experiment Station, Vicksburg, Miss. Tech. Bull. No. 5, 1961.

Ippen, A. T. and Harleman, D. R. F.: Two dimensional aspects of salinity intrusion in estuaries: analysis of salinity and velocity distributions., US Army Corps Eng., Comm. Tidal Hydraul., Tech. Bull. No. 13., 1967.

Kuijper, K. and van Rijn, L. C.: Analytical and numerical analysis of tides and salinities in estuaries; Part II: Salinity distributions in prismatic and convergent tidal channels, Ocean Dynam., 61, 1743–1765, 2011.

Langbein, W. B.: The hydraulic geometry of a shallow estuary, Int. Assoc. Scient. Hydrol. Bull., 8, 84–94, 1963.

Nguyen, A. D. and Savenije, H. H.: Salt intrusion in multi-channel estuaries: a case study in the Mekong Delta, Vietnam, Hydrol. Earth Syst. Sci., 10, 743–754, doi:10.5194/hess-10-743-2006, 2006.

Pethick, J.: An Introduction to Coastal Geomorphology, Edward Arnold Pub., London, 260 pp., 1984.

Rigter, B. P.: Minimum length of salt intrusion in estuaries, J. Hydr. Eng. Div.-ASCE, 99, 1475–1496, 1973.

Savenije, H. H. G.: A one-dimensional model for salinity intrusion in alluvial estuaries, J. Hydrol., 85, 87–109, 1986.

Savenije, H. H. G.: Salt intrusion model for high-water slack, lowwater slack, and mean tide on spread sheet, J. Hydrol., 107, 9–18, 1989.

Savenije, H. H. G.: Lagrangian solution of St. Venant's equations for alluvial estuary, J. Hydraul. Eng., 118, 1153–1163, 1992.

Savenije, H. H. G.: Composition and driving mechanisms of longitudinal tidal average salinity dispersion in estuaries, J. Hydrol., 144, 127–141, 1993a.

Savenije, H. H. G.: Predictive model for salt intrusion in estuaries, J. Hydrol., 148, 203–218, 1993b.

Savenije, H. H. G.: Salinity and Tides in Alluvial Estuaries, Elsevier, New York, 194 pp., 2005.

Savenije, H. H. G.: Salinity and Tides in Alluvial Estuaries, 2nd Edn., available at: http://salinityandtides.com/ (last access: 8 December 2014), 2012.

Schultz, E. A. and Simmons, H. B.: Fresh water-salt water density currents: a major cause of siltation in estuaries, in: Comm. Tidal Hydraul., Tech., Bull. No. 2, US Army Corps Eng., Vicksburg, MI, 1957.

Shaha, D. C. and Cho, Y.-K.: Comparison of empirical models with intensively observed data for prediction of salt intrusion in the Sumjin River estuary, Korea, Hydrol. Earth Syst. Sci., 13, 923–933, doi:10.5194/hess-13-923-2009, 2009.

Thatcher, M. and Harleman, D.: A mathematical model for the prediction of unsteady salinity intrusion in estuaries, in: R. M. Parsons Laboratory Report, No. 144, MIT, Cambridge, Massachusetts, 1972.

van der Burgh, P.: Ontwikkeling van een methode voor het voorspellen van zoutverdelingen in estuaria, kanalen en zeeen, Rijkwaterstaat Rapport, Rijkswaterstaat, 's-Gravenhage, 10–72, 1972.

Van Os, A. and Abraham, G.: Currents and Salt Intrusion, Lecture Note for the Hydraulic Engineering Course at IHE-Delft, Delft Hydraulics, Delft, 1990.

Van Rees, A. J. and Rigter, B. P.: Flume study on salinity intrusion in estuaries, Proc. Congr. Int. Assoc. Hydraul. Res. 13th, 303– 310, 1969.

Zhang, E., Savenije, H. H. G., Wu, H., Kong, Y., and Zhu, J.: Analytical solution for salt intrusion in the Yangtze Estuary, China, Estuar. Coast. Shelf S., 91, 492–501, 2011.

APPENDIX A
SAMPLE APPENDIX 1

Subbasin	*Stream length, km*	*Shape area, km²*	*Basin Slope*	*Tc*	*R*
W1380	36.61	30.31	28.12	8.93	12.13
W1330	35.38	27.90	19.62	10.48	14.05
W1300	33.84	23.88	18.65	10.50	14.18
W1290	12.82	3.17	14.63	5.96	8.89
W1280	48.57	54.65	29.75	10.61	13.98
W1270	22.99	12.93	16.76	8.23	11.40
W1260	27.43	13.23	19.67	8.96	12.58
W1250	56.76	47.36	10.65	21.10	26.91
W1240	57.50	44.01	17.95	16.54	21.76
W1230	45.67	37.28	26.40	11.12	14.96
W1220	30.32	20.26	15.44	10.61	14.30
W1210	41.66	23.28	10.22	17.44	23.11
W1200	46.22	33.41	7.38	21.77	27.76
W1190	29.52	18.20	13.44	11.24	15.15
W1180	52.88	55.25	25.33	12.47	16.35
W1170	43.45	28.35	17.67	13.43	18.04
W1160	23.11	7.20	5.62	15.45	21.20
W1150	43.57	57.02	46.97	7.55	10.09
W1370	27.06	18.73	29.60	6.90	9.61
W1130	40.74	30.94	11.89	15.28	19.95
W1120	18.18	8.43	13.96	7.59	10.65
W1110	28.84	17.85	10.88	12.26	16.37
W1100	17.50	8.16	31.93	4.83	7.06
W1090	23.73	14.38	28.91	6.36	8.97
W1080	10.85	3.43	7.62	7.01	10.00
W1070	12.02	2.54	3.06	12.73	17.85
W1060	37.97	22.33	28.84	9.47	13.19
W1050	47.52	45.33	13.11	16.10	20.66
W1040	40.55	24.36	7.41	19.90	25.85
W1030	21.39	7.89	3.81	17.29	23.04
W1020	16.58	5.86	6.25	10.91	15.07
W1010	38.33	27.29	9.47	16.42	21.35
W1000	38.89	36.12	24.62	9.92	13.23
W990	32.60	24.33	21.63	9.38	12.71
W980	50.97	42.01	20.42	13.88	18.35
W970	30.38	21.07	6.67	16.20	20.90
W960	46.53	33.44	28.66	11.00	14.99
W950	13.93	3.97	16.22	5.96	8.82
W940	49.31	38.90	12.90	17.13	22.25
W1320	36.05	21.89	7.37	18.05	23.51
W920	36.67	24.78	14.68	12.75	17.02
W910	4.19	0.46	7.85	3.53	5.63
W900	42.83	39.71	28.80	9.93	13.32
W890	39.63	36.29	24.09	10.21	13.61

W880	18.86	5.13	8.08	11.01	15.63
W870	38.64	32.73	8.97	16.65	21.30
W860	57.75	43.87	7.02	26.75	33.65
W850	28.35	8.29	3.51	23.46	31.40
W840	21.94	9.84	6.07	13.62	18.28
W830	32.23	23.09	6.49	17.19	22.06
W820	79.87	80.04	11.82	26.08	32.60
W810	30.01	23.32	13.66	10.99	14.57
W800	30.82	14.90	4.08	21.96	28.43
W790	21.02	6.84	7.52	12.24	17.03
W780	12.88	2.23	1.76	18.30	25.30
W770	38.46	21.67	1.96	37.62	46.11
W760	10.23	1.50	2.08	14.13	20.10
W750	58.55	56.54	2.07	48.81	56.80
W740	43.08	17.58	1.71	46.13	57.33
W730	87.89	80.87	6.14	39.78	48.32
W720	72.54	75.77	2.18	56.51	65.05
W710	27.24	20.01	24.11	7.65	10.50
W700	24.84	17.47	24.13	7.11	9.83
W690	28.72	19.16	8.78	13.50	17.74
W680	28.04	17.90	12.28	11.22	15.05
W670	19.97	7.54	18.55	7.29	10.50
W660	7.27	1.04	1.20	14.09	19.77

APPENDIX B
SAMPLE APPENDIX 2

Subbasin	Curve Number	Time of concentration (hr)	Storage Coefficient (hr)	Baseflow (m3/s)
W1380	39.64	8.93	12.13	0.11
W1330	36.61	10.48	14.05	0.62
W1300	44.10	10.50	14.18	1.31
W1290	45.01	5.96	8.89	1.39
W1280	39.63	10.61	13.98	1.28
W1270	38.02	8.23	11.40	1.44
W1260	45.93	8.96	12.58	4.53
W1250	44.06	21.10	26.91	4.79
W1240	47.19	16.54	21.76	1.29
W1230	48.23	11.12	14.96	3.52
W1220	52.60	10.61	14.30	0.16
W1210	47.48	17.44	23.11	1.54
W1200	58.11	21.77	27.76	0.22
W1190	47.43	11.24	15.15	0.57
W1180	53.49	12.47	16.35	1.12
W1170	53.15	13.43	18.04	1.64
W1160	39.30	15.45	21.20	4.74
W1150	53.41	7.55	10.09	1.63
W1370	45.27	6.90	9.61	0.78
W1130	41.26	15.28	19.95	0.68
W1120	39.93	7.59	10.65	2.83
W1110	46.54	12.26	16.37	2.20
W1100	42.09	4.83	7.06	0.45
W1090	42.54	6.36	8.97	2.40
W1080	44.15	7.01	10.00	2.60
W1070	30.75	12.73	17.85	0.06
W1060	45.87	9.47	13.19	1.73
W1050	46.77	16.10	20.66	1.56
W1040	43.67	19.90	25.85	2.55
W1030	49.46	17.29	23.04	0.36
W1020	41.53	10.91	15.07	2.24
W1010	43.93	16.42	21.35	1.51
W1000	41.33	9.92	13.23	2.73
W990	38.13	9.38	12.71	1.71
W980	37.91	13.88	18.35	2.40
W970	49.56	16.20	20.90	1.88
W960	45.32	11.00	14.99	0.50
W950	42.12	5.96	8.82	0.65
W940	40.04	17.13	22.25	1.71
W1320	41.35	18.05	23.51	2.91

W920	42.70	12.75	17.02	1.58
W910	36.89	3.53	5.63	0.25
W900	49.57	9.93	13.32	0.32
W890	38.27	10.21	13.61	1.09
W880	38.47	11.01	15.63	0.67
W870	47.62	16.65	21.30	1.31
W860	37.01	26.75	33.65	0.69
W850	46.65	23.46	31.40	2.10
W840	37.82	13.62	18.28	1.36
W830	37.99	17.19	22.06	3.55
W820	39.31	26.08	32.60	0.60
W810	46.07	10.99	14.57	1.95
W800	38.11	21.96	28.43	3.45
W790	43.59	12.24	17.03	1.33
W780	40.73	18.30	25.30	2.24
W770	45.19	37.62	46.11	1.64
W760	44.22	14.13	20.10	1.46
W750	40.25	48.81	56.80	2.46
W740	45.41	46.13	57.33	2.84
W730	49.27	39.78	48.32	3.02
W720	45.03	56.51	65.05	1.01
W710	50.85	7.65	10.50	0.99
W700	38.04	7.11	9.83	3.42
W690	43.51	13.50	17.74	0.30
W680	47.78	11.22	15.05	1.68
W670	40.14	7.29	10.50	1.92
W660	38.17	14.09	19.77	2.06